Soft Matter

Accepted Manuscript

This is an *Accepted Manuscript*, which has been through the Royal Society of Chemistry peer review process and has been accepted for publication.

Accepted Manuscripts are published online shortly after acceptance, before technical editing, formatting and proof reading. Using this free service, authors can make their results available to the community, in citable form, before we publish the edited article. We will replace this *Accepted Manuscript* with the edited and formatted *Advance Article* as soon as it is available.

You can find more information about *Accepted Manuscripts* in the Information for Authors.

Please note that technical editing may introduce minor changes to the text and/or graphics, which may alter content. The journal's standard Terms & Conditions and the Ethical guidelines still apply. In no event shall the Royal Society of Chemistry be held responsible for any errors or omissions in this *Accepted Manuscript* or any consequences arising from the use of any information it contains.

ROYAL SOCIETY OF CHEMISTRY

www.rsc.org/softmatter

Streaming Potential-Modulated Capillary Filling Dynamics of Immiscible Fluids

Aditya Bandopadhyay,[1] Shubhadeep Mandal,[2] and Suman Chakraborty[1,2*]

[1]Advanced Technology Development Center, Indian Institute of Technology Kharagpur, Kharagpur - 721302, India

[2]Department of Mechanical Engineering, Indian Institute of Technology Kharagpur, Kharagpur - 721302, India

The pressure driven transport of two immiscible electrolytes in a narrow channel with prescribed surface potential (zeta potential) is considered under the influence of a flow-induced electric field. The latter consideration is non-trivially and fundamentally different from the problem of electric field-driven motion (electroosmosis) of two immiscible electrolytes in a channel in a sense that in the former case, the genesis of the induced electric field, termed as streaming potential, is the advection of ions in the absence of any external electric field. As the flow occurs, one fluid displaces the other. Consequently, in cases where the conductivities of the two fluids differ, the imbibition alters the net conductivity of the channel, dynamically. We emphasize, through numerical simulations, that the alteration in the net conductivity has a significant impact on the contact line dynamics and the concomitant induced streaming potential. The results presented herein are expected to shed light on multiphase electrokinetics devices.

1. Introduction

The transport of two immiscible fluids where one phase displaces the other has been extensively studied in recent times, owing to a vast number of applications in lab-on-a-chip devices with implications in areas such as bio-fluid transport, mixing and other industrial and geophysical scenarios.[1–4] Analysis of such two phase flow processes may also hold the key to understanding the fundamental mass transport processes in plant vascular tissues, where osmotic pressure drives the flow of nutrients.[5,6] Understanding the imbibition dynamics in porous media has also been a focus of research owing to the possible applications in geological transport.[2,7–9] The aforementioned on-chip and reservoir-based applications are typically characterized by surfaces possessing a net charge owing to one of many possible mechanisms (thus leading to the formation of an electrical double layer (EDL)),[10,11] thereby enabling the prospect of flow control and modulation by means of electric fields.[12–15]

For single phase aqueous electrolytes in contact with charged surfaces, a vast body of literature exists with detailed expositions present for both electroosmosis (flow on account of an applied electric field) and streaming potential (induced electric field on account of a pressure gradient).[16–20] Das *et al.*[21] have shown in their analysis that the three phase contact line is nontrivially affected by the contributions of the free energy of the EDL and may lead to counterintuitive Cassie-Baxter transitions. Streaming potential, the focus of this work, develops in flows in which there is an induced electric field due to a pressure driven advection of the mobile part of the EDL.[12,22,23] The effect of the induced electric field is to

*email address for correspondence: suman@mech.iitkgp.ernet.in

Soft Matter Accepted Manuscript

retard the flow due to the pressure driven component, leading to an *electroviscous* retardation as observed in previous studies on both single phase flows [24–28] and capillary filling dynamics of two phase flows (the second phase being air or otherwise).[29–32] The extra resistance faced by a flow in the presence of streaming potential has been established by several earlier studies and has been referred to as the primary electroviscous effect (one may refer to the seminal book of Hunter[33]). It was shown that the accumulation of charges in the vicinity of the interface due to the presence of a charged substrate leads to insignificant amount of accumulation of charge for interfaces which are not dramatically curved (this may be violated for highly hydrophilic substrates). However, no studies have yet been reported in the literature on the streaming potential–modulated capillary imbibition dynamics of an immiscible binary system in which both the fluids contain ionic species.

Here, we consider streaming potential–mediated capillary filling dynamics of an immiscible binary electrolyte system.[2,7] For enhanced oil recovery and allied processes, one typically connects rock samples (which have an intricate network of nano-pores) to reservoirs of brine having different salinity, thereby causing a contrast in conductivity. Besides this, the simultaneous flow of multiple immiscible fluids may occur through rocks. Such porous media occur in the vadose zone for hydrocarbon extraction and so on.[2,7] The concerned physical scenarios with multiple phases contributing to the streaming potential are not well understood. Under these circumstances, the contribution of the two phases is commonly incorporated through an *ad-hoc* determination of wetting fractions and hydraulic conductivity of the capillaries, with an emphasis on the evaluation of the effective permeabilities and effective electrical conductivities of porous media.[34–37] However, the presence of a contact line between two immiscible phases leads to dramatically altered flow physics depending on the wettability of the walls. The associated problem of electroosmosis has been studied in the same context of an immiscible fluid displacing another, both containing electrolytes, under the action of an external electric field in a channel with charged walls.[38–40] However, no studies have yet been reported in the literature on the variable conductivity modulated contact line dynamics of an immiscible binary system subject to EDL phenomena. Bearing in mind that the magnitude of the induced electric field depends significantly on the nature of the conductivity of the displacing fluid and the displaced fluid, one may infer that the resistance faced by the column of liquids being driven through the channel during capillarity induced motion due to the induced electric field depends on the relative conductivities of the two fluid as well as the location of the interface, i.e. the extent of filling of the incipient fluid.

Towards analyzing such scenarios, we consider a channel with a uniform zeta potential with two reservoirs having different bulk concentrations (please see figure 1). Owing to the different bulk concentrations, the thickness of the EDL varies across the two liquids and is typically of the order of 10 - 100 nm.[12] The EDL properties and the bulk ionic conductivity are functions of the reservoir ionic concentrations. Depending on the location of the contact line (which itself depends on the nature of the induced electric field), the net ionic conductivity of the channel differs, thereby resulting in a complicated time dependent

Soft Matter Accepted Manuscript

contact-line dynamics mediated by the induced streaming potential. We model the complex dynamics through a phase field model coupled with electrohydrodynamics which accounts for the retarding body force (leading to electroviscous effects) due to the induced streaming potential.

2. Mathematical formulation

2.1 System description and governing equations

We consider a parallel plate channel of height H consisting of two immiscible fluids. The two ends of the channel are connected to two reservoirs which may have, in general, different bulk ionic concentrations. A favourable pressure gradient acts in such a way to drive the flow from the left reservoir to the right. The contact angle at the solid-liquid-liquid interface is denoted by θ_s. The surface potential at the wall is denoted by ζ and the electrical potential due to this is denoted by ψ_i (the subscript denotes the i^{th} fluid). Briefly, the overall transport process may be summarized as follows. The attraction of counterions towards the charged walls leads to a net charge density in the fluids which, when driven by an external pressure gradient, leads to the generation of an advective current known as streaming current. There is no external electric field acting on the system which implies that the total current must be zero. As a consequence, there must be an induced electric field E_{ind} (due to accumulation of the net charge density downstream due to the flow) which causes the conduction current to exactly balance the streaming current.

The transverse potential distribution, ψ_i, due to the surface charge is described by the Poisson equation [10]

$$\nabla\cdot\left(\varepsilon_i\nabla\psi_i\right) = -\rho_{e,i} = -\left(z_{i,+}n_{i,+} + z_{i,-}n_{i,-}\right)e; \qquad i = 1,2. \tag{1}$$

where ε_i and $\rho_{e,i}$ represent electrical permittivity and electrical charge density of i^{th} fluid respectively. The electrical charge density $\rho_{e,i}$ can be expressed in terms of number density $\left(n_i\right)$ and valence $\left(z_i\right)$ of cationic and anionic species. For the two fluids $\left(i = 1,2\right)$, the permittivity $\left(\varepsilon_i\right)$ and bulk ionic concentration $\left(n_{i,0}\right)$ need not be same and we assume that the two columns of fluid are connected to different reservoirs (please see figure 1). We consider that the Boltzmann distribution [12] of ionic species prevails in the individual phases $n_{i,\pm} = n_{i,0}\exp\left(\mp z_{i,\pm}e\psi_i / k_BT\right)$. Briefly, the Boltzmann distribution may be justified in cases where the Péclet number $\mathrm{Pe} = U_{ref}H/D$ is small (U_{ref} is the characteristic velocity, H is the channel height and D is the ionic diffusivity), thereby leading to a balance of diffusion and electromigration, consequently leading to the above ionic distribution. Typically,

Soft Matter Accepted Manuscript

$D \sim 10^{-9}\ \mathrm{m^2 s^{-1}}$, $U_{ref} \sim 10^{-4}\ \mathrm{ms^{-1}}$ and $H \sim 10^{-7}\ \mathrm{m}$ lead to $\mathrm{Pe} = 10^{-2}$, thereby justifying neglecting the advective component of the ionic flux.[41]

For simplicity, we choose a symmetric binary solution in both the fluids with $z_{i,+} = -z_{i,-} = z$. We combine the Boltzmann distribution with the Poisson equation, along with the introduction of the following normalization parameters: $\bar{\psi} = ze\psi / k_B T$, $\bar{\mathbf{x}} = \mathbf{x} / H$, $\bar{\kappa}_i = \kappa_i H = \left(\sqrt{\frac{2z^2 e^2 n_0}{\varepsilon_i k_B T}} \right) H$, to yield

$$\bar{\nabla}^2 \bar{\psi}_i = \bar{\kappa}_i^2 \sinh\left(\bar{\psi}_i\right). \tag{2}$$

Equation (2) satisfies $\bar{\psi} = \bar{\zeta}$ at the top and bottom walls of the channel, and no-penetration boundary condition at the inlet (left boundary) and outlet (right boundary) of the channel, i.e., $\partial \bar{\psi} / \partial \bar{x} = 0$ at $\bar{x} = 0, \bar{L}$ (where $\bar{L}$ is the non-dimensional length of channel). The potential and the normal gradient of $\bar{\psi}$ are continuous across the interface, i.e., at Γ (the interface), $\left[\bar{\psi}_i\right] = 0$ and $\left[\nabla \bar{\psi}_i \cdot \mathbf{n}\right] = 0$ where $\mathbf{n}$ is the unit normal pointing from fluid 1 to 2 and $\left[\alpha_i\right]$ at the interface represents $\alpha_2 - \alpha_1$.

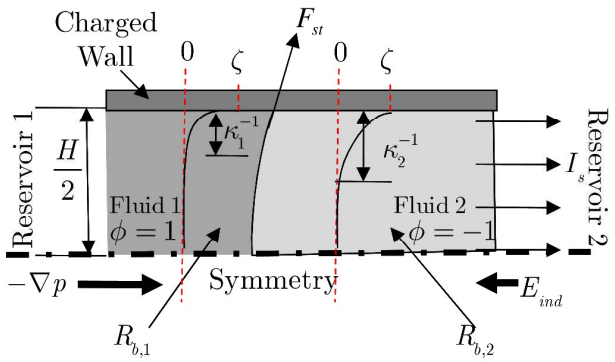

FIG. 1. Schematic depicting the nature of capillary filling for two immiscible fluids. The fluids are respectively denoted by $\phi = 1$ and $\phi = -1$. The fluid to the left is connected to reservoir 1 and the fluid to the right is connected to reservoir 2 whose bulk concentrations are, in general, not equal. Owing to different bulk concentrations, the bulk resistivity (or equivalently, the inverse of conductivity) of the two fluid columns, denoted by $R_{b,1}$ and $R_{b,2}$, are different while the characteristic electrical double layer thickness, denoted by κ_1^{-1} and κ_2^{-1} are also different (please refer to equation (2)). The interface is acted upon by the surface tension force while a pressure gradient drives the flow from left to right. The presence of bulk mobile charges in conjunction with overall electroneutrality induces an electric field which opposes the pressure driven flow. A pressure gradient $-\nabla p$ acts from the left to right reservoir while the induced streaming electric field E_{ind} acts from the right to the left.

Soft Matter Accepted Manuscript

The presence of mobile charges in the fluids leads to interesting electrokinetic phenomena which have been well addressed for single-phase flows. The advection current is balanced by an equal and opposite current. This reverse current, known as the conduction current, is driven by the induced streaming potential and is responsible for an additional body force acting on the fluid in the direction opposite to that of the pressure driven flow. Thus, under the weak-field approximation, the induced axial electric potential $\left(\psi^*\right)$ satisfies the Laplace equation [10]

$$\bar{\nabla}^2\bar{\psi}^* = 0, \tag{3}$$

where the dimensionless streaming potential is given as $\bar{\psi}^* = \psi^* / \psi_{ref}$; ψ_{ref} is determined later on from the momentum equation. Equation (3) satisfies $\partial\psi^* / \partial\bar{y} = 0$ at the top and bottom walls. For convention, we take the inlet to be at a reference ground potential $\bar{\psi}^* = 0$ and the outlet to be at a dimensionless potential $\bar{\psi}^* = \bar{V}_s$ ($\bar{V}_s$ denoting the induced streaming potential with reference to a ground left electrode). The magnitude of $\bar{V}_s$ will be determined later in a consistent fashion by making use of the electroneutrality constraint.

Here, we employ the phase field model to capture the multiphase electrohydrodynamics.[42] The flow field is determined by the Navier-Stokes equations along with the continuity equation, with due accounting for the capillary stress as well as the Maxwell stress. In dimensional form, the Navier-Stokes equation for an incompressible Newtonian fluid can be written as [43]

$$\rho_i \frac{D\mathbf{u}}{Dt} = -\nabla p + \nabla\cdot\left\{\eta_i\left(\nabla\mathbf{u} + \left(\nabla\mathbf{u}\right)^T\right)\right\} + \mu\nabla\phi + \rho_{e,i}\mathbf{E} - \frac{1}{2}\left(\mathbf{E}_t\cdot\mathbf{E}_t\right)\nabla\varepsilon; \qquad i = 1,2 \tag{4}$$

where $\mathbf{u} = \left(u, v\right)$ represents the velocity vector, p represents the pressure; ρ_i, η_i and $\rho_{e,i}$ represent the density, viscosity and charge density of the i^{th} fluid. $\mathbf{E}$ represents the induced streaming electric field, $\mathbf{E}_t$ represents the total electric field (field due to the presence of EDL and induced streaming potential), μ and ϕ denote the chemical potential and phase field parameter (which we shall elaborate in the next section; in essence, $\phi = 1$ denotes one phase and $\phi = -1$ denotes the other phase). The first two terms in the right hand side can be identified as the contribution from the hydrodynamic stresses. The third term represents the effect of the surface tension which exists only in a very thin region near the interface of the fluid since $\nabla\phi$ is non-zero only at the interface. The fourth term represents the body force acting on the mobile part of the EDL while the last term represents the polarization force due to a mismatch in the permittivity of the two fluids. In our analysis, for simplicity, we neglect

Soft Matter Accepted Manuscript

the last term and only focus on the effects of the streaming potential through the force acting on the mobile charges. In a non-dimensional form we can write equation (4) as

$$\bar{\rho}\,\mathrm{Re}\frac{D\bar{\mathbf{u}}}{D\bar{t}} = -\bar{\nabla}\bar{p} + \bar{\nabla}\cdot\left\{\bar{\eta}\left(\bar{\nabla}\bar{\mathbf{u}} + \left(\bar{\nabla}\bar{\mathbf{u}}\right)^{T}\right)\right\} + \frac{1}{\mathrm{CaCn}}\bar{\mu}\bar{\nabla}\phi - \frac{\bar{\varepsilon}}{\bar{\eta}}\bar{\mathbf{E}}\bar{\kappa}_r^2\sinh\bar{\psi}_r, \tag{5}$$

where $\bar{\rho}$ depicts the density of the fluid in terms of the order parameter given by $\bar{\rho} = \left(\frac{1+\phi}{2}\right) + \left(\frac{1-\phi}{2}\right)\frac{\rho_2}{\rho_1}$ and similarly $\bar{\eta} = \left(\frac{1+\phi}{2}\right) + \left(\frac{1-\phi}{2}\right)\frac{\eta_2}{\eta_1}$.[42,44] The parameter $\bar{\kappa}_r$ highlights the fact that the dimensionless thickness of EDL should also be taken to be a function of the order parameter given by $\bar{\kappa}_r^2 = \left(\frac{1+\phi}{2}\right) + \left(\frac{1-\phi}{2}\right)\frac{\bar{\kappa}_2^2}{\bar{\kappa}_1^2}$. The dimensionless velocity $\bar{\mathbf{u}}$ is given by $\mathbf{u}/U_{ref}$, the pressure gradient is made dimensionless by the applied pressure gradient which is typically in the order of 10^8 Pa/m for micro and nano-channel experiments [45]. Thus, the reference velocity is determined from the pressure driven transport and is given by $U_{ref} = \left(\nabla p\right)_{ref} H^2/\eta_1$. Similarly, the dimensionless induced electric field $\bar{\mathbf{E}} = \mathbf{E}/E_{ref}$ is derived by setting $E_{ref} = U_{ref}/\left(\varepsilon_1 k_B T/ze\eta_1\right)$. In a dimensionless form, the reference electric field can be associated with the reference potential as $\psi_{ref}^{*} = E_{ref}\bar{L}$; $\bar{L}$ being the dimensionless length of the channel. The Reynolds number is given as $\mathrm{Re} = \rho_1 U_{ref} H/\eta_1$, the capillary number is defined as $\mathrm{Ca} = \eta_1 U_{ref}/\gamma$ and the Cahn number $\mathrm{Cn} = \xi/H$; ξ being the characteristic thickness of the interface (the details of the phase-field model and its non-dimensionalization are presented below).

2.2 Phase field equations

To numerically simulate the present two phase electrokinetic flow with contact line motion, we use the phase field model. The advantages of using this, aptly termed, diffuse-interface model are: it is thermodynamically consistent, there is no need to track the interface explicitly and there is no strict requirement to specify the slip condition at the contact line.[43,46–49] Under the framework of phase field model, the state of a system having two immiscible phases can be represented by a scalar parameter $\phi\left(\mathbf{x},t\right)$ which is known as phase field order parameter. In our analysis we have considered $\phi = 1$ for fluid 1 and $\phi = -1$ for fluid 2; the interface is represented by $\phi \in \left(-1,1\right)$, noting that ϕ varies rapidly in the region of the interface. The Ginzburg-Landau free energy of a two phase system can be expressed as a functional of phase field order parameter of the following form [42,50]

$$F\left[\phi\right] = \int_{\Omega}\left[f\left(\phi\right) + K\frac{\left|\nabla\phi\right|^2}{2}\right]d\Omega, \tag{6}$$

Soft Matter Accepted Manuscript

where Ω is the total domain of interest. The term $f(\phi)$ denotes the free energy density of the homogeneous system far away from the interface which may be further expressed in terms of the phase field order parameter by using a double-well potential as $f(\varphi) = A(\varphi^2 - 1)^2 / 4$. The term $K|\nabla\varphi|^2/2$ denotes the interfacial free energy density which is nonzero in the diffuse interfacial region only. The bulk free energy coefficient (A) and interfacial free energy coefficient (K) are related to interfacial thickness (ξ) of the diffuse interface and the surface tension coefficient (γ) between the two phases through $A \sim \gamma/\xi$, $K \sim \gamma\xi$.

The dynamic evolution of phase field order parameter can be given in a conservative form by the Cahn-Hilliard equation as [42,47]

$$\frac{\partial\phi}{\partial t} + \mathbf{u}\cdot\nabla\phi = \nabla\cdot(M\nabla\mu), \tag{7}$$

where M denotes the mobility of the order parameter which is taken as constant for the present analysis. The term on the right hand side of equation (7) is responsible for the diffusion of the phase field order parameter and hence is focal in alleviating the contact-line stress singularity. The chemical potential μ can be obtained by performing a variational derivative of the free energy of the system of the following form

$$\mu = \frac{\delta F}{\delta\phi} = \frac{\gamma}{\xi}\left[\left(\phi^3 - \phi\right) - \xi^2\nabla^2\phi\right]. \tag{8}$$

In a non-dimensional sense, the complete description of the Cahn-Hilliard equation is given by

$$\begin{aligned} &\frac{\partial\phi}{\partial\bar{t}} + \bar{\mathbf{u}}\cdot\bar{\nabla}\phi = \frac{1}{\mathrm{Pe}}\bar{\nabla}^2\bar{\mu}, \\ &\bar{\mu} = \phi^3 - \phi - \mathrm{Cn}^2\nabla^2\phi. \end{aligned} \tag{9}$$

Here, $\mathrm{Pe} = H^2U_{ref}/M\sigma$ is the Péclet number which controls the diffusion of order parameter as compared to the advection, whereas the Cahn number (Cn) represents the normalised interface thickness. The boundary conditions at the walls of the channel required to solve equation (9) is of the following form

$$\begin{aligned} &\mathbf{n}\cdot\nabla\mu = 0, \\ &\mathbf{n}\cdot\nabla\phi = -\tan\left(\frac{\pi}{2} - \theta_s\right)\left|\nabla\phi - (\mathbf{n}\cdot\nabla\phi)\mathbf{n}\right|, \end{aligned} \tag{10}$$

Soft Matter Accepted Manuscript

where θ_s is the specified contact angle on the channel walls and **n** denotes the direction of the unit normal away from the wall. Thus, the complete description of the hydrodynamics, and the electric field, is given by equations (5) and (9) with the appropriate boundary conditions.

2.3 Evaluation of net channel electrical resistance

In our discussions made so far, the description of the streaming electric field and streaming potential remain unaddressed. In order to address the related consequences, we appeal to the overall electroneutrality condition for estimating the induced potential. The electroneutrality condition implies that in the absence of an induced electric field, the sum of streaming current and conduction current must be zero:

$$\int_{-H/2}^{H/2} \rho_e u dy = \frac{V_s}{R}, \tag{11}$$

where V_s denotes the back-potential difference induced across the channel (since it is assumed that the left electrode is at a zero potential, V_s denotes the potential of the right electrode), R denotes the total electrical resistance of the channel and the left hand side of equation (11) represents the current flux at the exit boundary. The total resistance of the channel comprises of two contributions: (a) the conductivity of the bulk fluid and (b) the conductivity of the Stern layer. Typically calculations are done by disregarding the Stern layer conductivity, but we account for it since we later show that it plays a major role in the overall description of the electrokinetic phenomenon. The Stern layer and the bulk resistances are in parallel which implies that the total resistance may be written as $1/R = 1/R_b + 1/R_s$; R being the total resistance, R_b being the bulk resistance and R_s being the Stern layer resistance. The Stern layer resistance may be written as $1/R_s = \sigma_s / L$; L is the length of the channel and σ_s is the conductivity of the Stern layer.[51,52] The bulk resistance may be evaluated by $R_b = \int_0^L \frac{dx}{\int_{-H/2}^{H/2} \sigma dy}$ where σ is the conductivity of the bulk which is given by $\frac{2z^2e^2n_{0,i}\cosh\bar{\psi}}{f}$; f being the ionic friction factor. The nature of the bulk conductivity dictates that as the potential drops to zero in the bulk, the conductivity tends to a bulk conductivity given by $\sigma_b = \frac{2z^2e^2n_{0,i}}{f}$. This results in an integral form of the fluid electrical

Soft Matter Accepted Manuscript

resistance of the channel given by $R_b = \left(\frac{2z^2e^2n_{0,i}}{f} \right)^{-1} \int_0^{\bar{L}} \frac{d\bar{x}}{\int_{-1/2}^{1/2} \cosh \bar{\psi} d\bar{y}}$. The total resistance of the channel is thus

$$\frac{1}{R} = \frac{2z^2e^2n_{0,i}}{f} \left\{ \left(\int_0^{\bar{L}} \frac{d\bar{x}}{\int_{-1/2}^{1/2} \cosh \bar{\psi} d\bar{y}} \right)^{-1} + \frac{\mathrm{Du}}{\bar{L}} \right\} = \frac{2z^2e^2n_{0,i}}{f} \frac{1}{\bar{R}}, \tag{12}$$

where $\mathrm{Du} = \sigma_s / H\sigma_b$ represents the Dukhin number and it signifies the ratio of the Stern layer conductivity to the bulk conductivity. Therefore, the dimensionless form of the electroneutrality condition may be written as

$$\bar{V}_s = \frac{V_s}{\psi^*_{ref}} = -J \frac{1}{\bar{L}} \bar{\zeta} \bar{R} \int_{-1/2}^{1/2} \bar{u} \sinh \bar{\psi}_2 d\bar{y} \tag{13}$$

where $J = \left\{ \frac{\varepsilon_1 k_B T}{\eta_1 z^2 e^2} f \right\}$ represents the characteristic ratio of the magnitude of the streaming current to the current due to conduction.

The above methodology for evaluating the induced streaming potential, as compared against the traditionally employed method, accounts for the fact that the channel is not simply occupied by one single fluid phase. The classical approach, on the other hand, is to balance the streaming current as evaluated in equation (11) by the conduction current, which is traditionally taken to be *invariant* along the channel axis (unlike the reality in case of a two-fluid system having different ionic concentrations of the constituent phases). The result of this simplification employed in the classical literature is the elimination of the long and tedious integral in the evaluation of the electrical resistance of the channel, $R_b = \left(\frac{2z^2e^2n_{0,i}}{f} \right)^{-1} \int_0^{\bar{L}} \frac{d\bar{x}}{\int_{-1/2}^{1/2} \cosh \bar{\psi} d\bar{y}}$ to yield $R_b = \left(\frac{2z^2e^2n_{0,i}}{f} \right)^{-1} \frac{L}{\int_{-1/2}^{1/2} \cosh \bar{\psi} d\bar{y}}$. This significantly simplifies the evaluation of the streaming potential. Note that equation (12) would then yield $\frac{1}{\bar{R}} = \left\{ \frac{\int_{-1/2}^{1/2} \cosh \bar{\psi} d\bar{y}}{\bar{L}} + \frac{\mathrm{Du}}{\bar{L}} \right\}$. Further simplification that the surface conductivity is negligible as compared to the bulk conductivity (Du → 0) implies that $\frac{1}{\bar{R}} = \frac{\int_{-1/2}^{1/2} \cosh \bar{\psi} d\bar{y}}{\bar{L}}$ and consequently, from equation (13) we can find a simplified version of

Soft Matter Accepted Manuscript

the potential as $\bar{V}_s = -J\bar{\zeta}\dfrac{\int_{-1/2}^{1/2}\bar{u}\sinh\bar{\psi}_2 d\bar{y}}{\int_{-1/2}^{1/2}\cosh\bar{\psi}d\bar{y}}$. This result has been widely employed for routine streaming potential calculations, but loses its validity in a strict sense for a binary system with different ionic conductivities of the constituent fluids.

3. Results and discussions

Before presenting the effects of different governing parameters on the contact line dynamics and subsequent alteration in streaming potential, we validate the present diffuse interface numerical model with that of Yue et al.[47] The phase field model (or more specifically the Cahn-Hilliard model) replaces the macroscopic sharp interface by a diffuse one. Incorporation of this diffuse interface removes the singularity at the contact line and there is no requirement of specifying the slip at the contact line explicitly.[48] However, the implementation of the Cahn-Hilliard model introduces two non-dimensional numbers which are otherwise absent in sharp interface formulations, namely the Cahn number $\mathrm{Cn} = \xi/H$ and the Péclet number $\mathrm{Pe} = H^2 U_{ref}/M\sigma$ or equivalently, as defined by Yue et al.[47] $\mathrm{S} = \sqrt{M\eta_2}/H$. The thickness of the fluid-fluid interface is governed by Cn, while the diffusion of the order parameter is governed by Pe (or S). For multiphase flows without the presence of contact lines, converged results can be obtained using the Cahn-Hilliard model only when the results are independent of interface thickness (i.e. Cn independence has been achieved). It has been established through numerical simulations[49] that $\mathrm{Cn} = O\left(10^{-2}\right)$ gives results which are independent of interface thickness and well matches with the sharp interface limit. As actual fluid-fluid interface thicknesses are of $O\left(10^{-9}\right)$, i.e. a few molecular diameters wide, in practice we employ much thicker interface to render the problem computationally feasible. To compensate for this artificially thick interface thickness, it is customary to adjust the diffusion of the order parameter arising in the Cahn-Hilliard equation by properly specifying Pe. Thus, when the contact line is absent, the Cahn-Hilliard diffusion has very little role to play on the interfacial dynamics. However, the Cahn-Hilliard diffusion which is governed by the gradient of chemical potential, plays a major role towards determining the contact line speed and the dynamic contact angle when the contact line is present in the multiphase systems. Hence, proper choices of Cn and Pe (or equivalently S) is of utmost important in moving contact line problems. Yue et al.[47] have performed both numerical simulations and scaling analysis and established that there is a threshold value of Cn for fixed values of other parameters to reach sharp interface limit in the presence of moving contact line. The recommended guideline for the upper limit of Cn is

$$\mathrm{Cn}_{\mathrm{threshold}} = 4\mathrm{S}, \tag{1.14}$$

Soft Matter Accepted Manuscript

where both the liquids have same viscosity. Thus, following their guideline, we consider $S = 0.01$ and a corresponding $Cn = 0.02$ which is well below $Cn_{threshold}$. We consider a 2D rectangular computational domain of length $4H$. The top and bottom walls are moving with constant velocity but in opposite directions. The liquid-liquid interface at steady state is shown in figure 2 for the parameters specified in the figure caption. Here we consider triangular grids of size $\Delta h = Cn/2$. The phase field formalism with coupled hydrodynamics has been solved in the finite element framework of COMSOL™. Figure 2 depicts that for $Ca = 0.01$ and 0.02 our numerical computations are in excellent agreement with that of Yue et al.[47]

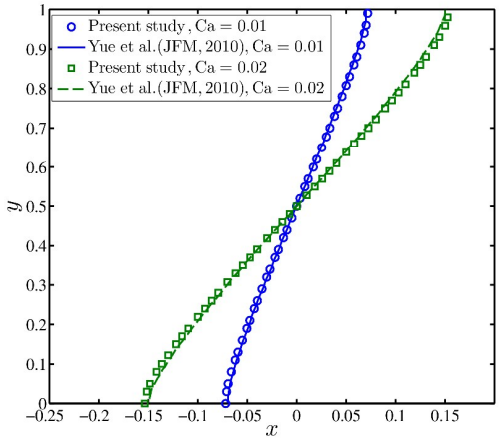

FIG. 2. Steady state interface shape in Couette flow for $Ca = 0.01, 0.02$ and $\theta_s = \pi/2$. Other parameters have the following values: Cn=0.02 and $\lambda = 1$. In accordance with Yue et al.[47] we consider $Pe = CaCn/S^2$ with $S = 0.01$.

To study the current problem, we consider a 2D rectangular computational domain of length $5H$ and exploiting the symmetry of the problem we have used height of the computational domain $H/2$. We consider $Cn = 0.02$ with triangular grids of size $\Delta h = Cn/2$ and $S = 0.01$ for all the simulations. From a pumping perspective, it is of utmost interest to observe the rate of filling into the capillary and how it is affected by the contrast in conductivities of the two fluids as quantified by the temporal evolution of the spatial location of the contact-line. Apart from this, from an electrokinetic perspective, the magnitude of the induced streaming potential is of great interest as it is an indicator of the extra resistance faced by the flow. As mentioned earlier and as we shall observe below, the conductivities of the two fluids plays a vital role towards the modulation of the contact line velocity, while the electrokinetic parameters such as the zeta potential and surface conductivity also explicitly affect the nature of the filling. In the discussion below, unless specifically mentioned, the Dukhin number is considered to be 0. The ionic friction factor is determined by utilizing the Stokes drag acting on an ion as $f = 6\pi\eta_1 a_{ion}$ where the ionic radius is taken to be 0.3 nm. For typical magnitudes of the parameters chosen to be: $\varepsilon_1 \sim 60 \times 8.85 \times 10^{-12}\ \mathrm{F\,m^{-1}}$,

Soft Matter Accepted Manuscript

$k_B = 1.38\times10^{-23}\,\mathrm{m^2\,kg\,s^{-2}\,K^{-1}}$, $T \sim 300\,\mathrm{K}$, $\eta_1 \sim 10^{-3}\,\mathrm{Pa\,s}$ while the ionic friction factor is given by $f = 6\pi\eta_1 a_{ion}$ with $a_{ion} \sim 0.3\,\mathrm{nm}$, we obtain the dimensionless parameter to be $O(0.1)-O(1)$. In order to account for the average permittivity across the channel, the relative permittivity has been taken to be 60. In all the results presented here, we consider a contact angle of 60°.

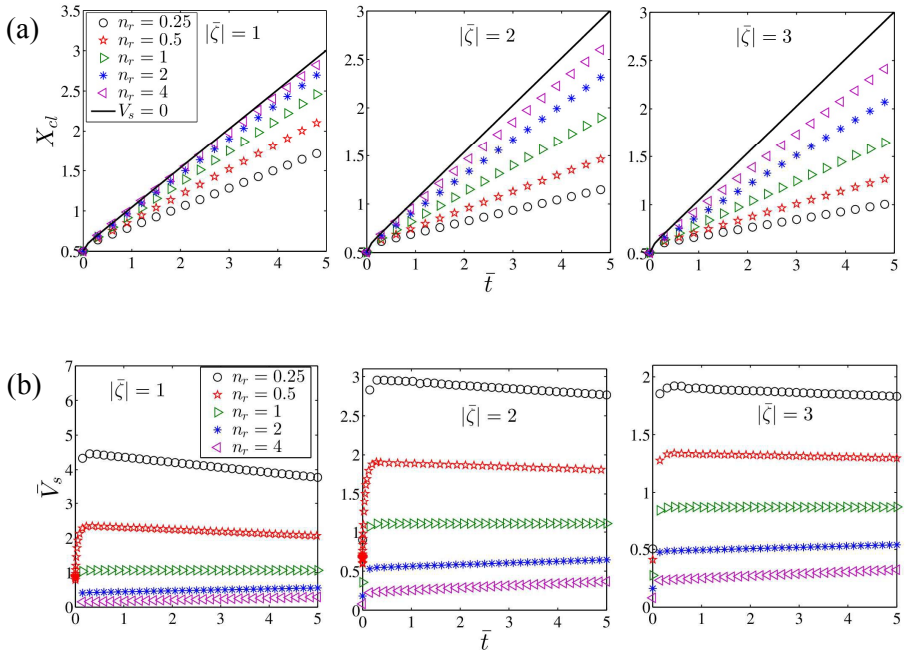

FIG. 3. (a) Temporal variation of the contact line location, X_{cl}, for various n_r and (b) temporal variation of the induced streaming potential, $\bar{V}_s$ plotted for various n_r and for different $|\bar{\zeta}|$ (1, 2 and 3). Here we have considered $\mathrm{Ca} = 0.03$ and $\theta_s = \pi/3$. The solid line in figure 3a represents the capillary filling characteristic for the case where the streaming effects are absent altogether (undamped case).

From figures 3a and 3b, the effect of the temporal evolution in filling length (equivalently, the penetration distance of the contact line into the capillary, i.e. the positive x direction) and streaming potential due to various values of n_r is clear. At a given time instant, the penetration length of the capillary increases as n_r increases. $n_r > 1$ implies that the second fluid (fluid on the right in figure 1) has a higher bulk conductivity and, associated with this, a thinner EDL as compared to the first fluid. Therefore as the first fluid displaces the second fluid, the net bulk conductance of the channel tends to decrease, leading to an increase in the induced electric field as more of the fluid starts to penetrate the channel. Conversely, for $n_r <$ 1 the trend reverses; as the capillary fills the channel, the conductance of the channel increases which leads to a gradual decrease in the induced electric potential, except for the initial rapid transience region during the start up of the flow. The effect of n_r is due to two

Soft Matter Accepted Manuscript

separate phenomena - the first being the higher streaming current at the exit of the channel for small n_r (a lower concentration leads to a thicker EDL and a larger current flux at the exit of the channel) and the second factor being the lower conductivity of the liquid column (as seen from the expression for the bulk conductivity equation (12)). The effect of the magnitude of zeta potential on the filling characteristics is not entirely straightforward and we shall discuss this later in this section.

Presently, we note that the higher magnitude of zeta potential leads to a larger streaming current while at the same time this larger induced electric field leads to a larger retardation force on the fluid. This results in a lower imbibition velocity as the zeta potential is increased; this leads to a decreased capillary penetration into the channel. The end effect of these feedback-like characteristics is that as the zeta potential is increased, the magnitude of the induced electric field drops. The case $n_r = 1$ is reminiscent of the case where the effect of the interface is to only induce a capillary pressure across the interface maintaining the other properties to be identical. For $n_r < 1$, in the early regimes of filling, we have a fluid with lower conductivity which occupies the larger length of the channel (please refer to figure 1 for a schematic description). This leads to an initially large induced streaming potential. Quite naturally, as fluid 1 begins to displace fluid 2, the induced field begins decreasing on account of the higher conductivity of the incipient fluid. The effect of increasing the zeta potential is to reduce the induced streaming potential. One thing to note here is that for all cases presented above, the filling length at a particular time is always smaller than the filling length in the absence of streaming potential ($\bar{V}_s$=0) thus highlighting the underpinning electroviscous damping.

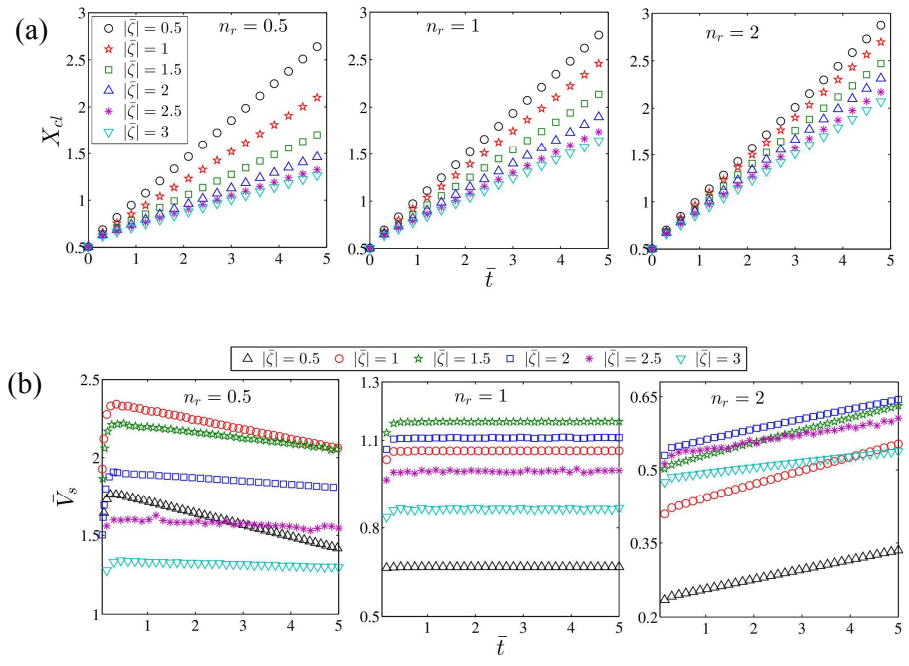

Soft Matter Accepted Manuscript

FIG. 4. (a) Temporal variation of the contact line location and (b) temporal variation of the induced streaming potential plotted for various $|\bar{\zeta}|$ and for different n_r (0.5, 1.0 and 2.0). Here we have considered $\mathrm{Ca} = 0.03$, and $\theta_s = \pi/3$.

Unlike n_r, the zeta potential is an intrinsic property of the substrate and exerts a significant influence on the flow behaviour. In figures 4a and 4b, we depict the temporal evolution of the filling length for different surface zeta potentials and for three different n_r (0.5, 1.0 and 2.0). The surface potential (or similarly surface charge density) is typically dictated by various chemical factors including the solution pH and other chemical equilibrium conditions at the surface. As a result, for various porous media, the magnitude of surface potential may vary from as low as ~ 20 mV to as high as 200 mV. Beyond the implicit nature of manifestation of the n_r, we now observe the various implications of the zeta potential on the flow. Like n_r, the effect of the zeta potential is also two-fold. One is through the EDL distribution which directly affects the streaming current flux at the exit of the channel and the other is through the alteration in the ionic number density which leads to an altered conductivity. For example, a higher surface potential leads to a larger potential throughout the channel as compared to a rapid decay to a zero centerline potential. This leads to a higher flux in the streaming current. At the same time, it also leads to larger variation in the conductivity which yields an enhanced streaming potential. We note that the variation need not be monotonic i.e. there exists a certain zeta potential at which the induced streaming potential is maximum. The trends observed through figure 4 are that as the magnitude of the zeta potential is increased, the induced streaming potential initially increases, reaches a peak, and then begins decreasing. Note, however, that the trends in the penetration length, unlike the induced streaming potential, are monotonic. The penetration distance, as verified through figure 4 decreases with an increase in the magnitude of the zeta potential; the extent of decrease is smaller as the potential increases. Quite intuitively, a higher n_r leads to a faster filling, thus corroborating with the observations of figure 3.

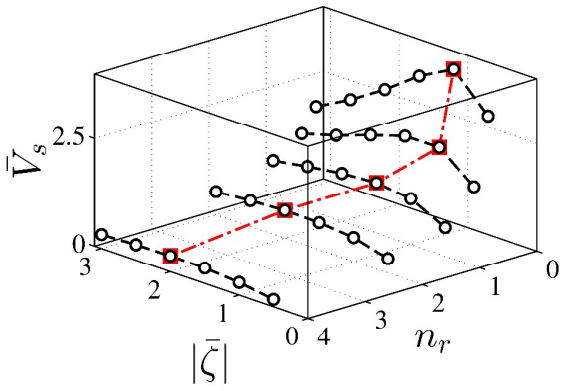

FIG. 5. Variation of the dimensionless streaming potential $\bar{V}_s$ evaluated at $\bar{t}$ = 5 as a function of the ζ potential and n_r. The location of the maxima in the streaming potential for a fixed n_r is represented using the red

Soft Matter Accepted Manuscript

filled square marker while the locus of the maxima is denoted via the dash-dot line. Here we have considered Ca=0.03 and $\theta_s = \pi/3$.

In order to establish the nature of the variation of long time streaming potential for both variations of n_r and ζ, we plot the $\overline{V}_s$ at an arbitrary time $\overline{t} = 5$ for different n_r and different zeta potentials in figure 5. For a fixed n_r, it is observed that there is a maxima in the induced streaming potential as the zeta potential magnitude is increased. Remarkably, as the n_r increases, the magnitude of zeta potential at which the maximum occurs (open circle marker) increases, while noting that the magnitude of the maximum streaming potential decreases as n_r increases. This implies that the impact of the n_r is quite severely manifested in the case of small n_r , i.e., a higher conducting fluid displacing a lower conducting fluid leads to larger manifestation of electrokinetic effects. As noted earlier, the impact of ζ on the streaming current is through the effect on the potential profile, i.e., a larger ζ would lead to a larger net charge density in the channel and, therefore, be expected to yield a larger advective flux of ions. Only accounting for the effect of zeta potential on the streaming current would imply that the increase in the streaming current would need to be balanced by a larger induced electric field, whereby we should be able to observe only a monotonous increase without any maxima in the streaming potential (at a fixed n_r). However, it was noted that the conductivity of the fluids is also dictated by the potential distribution and that the increase in the ζ potential also leads to an increase in the fluid conductivity (similar trends have also been highlighted in earlier works[53]). Thus, if the fluid conductivity also increases, the induced streaming potential may increase or decrease, depending on the relative increase of the streaming current and fluid conductivity. When the fluid conductivity increases more rapidly than the streaming current upon the increase in the ζ potential, the streaming potential decreases and vice-versa. Therefore, at a specified n_r, as the ζ potential is increased, initially the streaming current increases at a faster rate than the conductivity, thereby leading to an increase in the streaming potential. After attaining the maxima, the trends then reverse. At a lower n_r, we observe that the capillary filling is significantly slower than that at higher n_r. Thus, for $n_r < 1$, the channel is still mostly occupied by a lower conductivity fluid as compared to the case when $n_r > 1$. The lower conductivity fluid, quite naturally, leads to a higher streaming potential. Interestingly, the effect of zeta potential is significantly more prominent for $n_r < 1$. In other words, the streaming potential is more sensitive to the changes in the ζ potential at low n_r. For $n_r > 1$, the channel has an already larger conducting fluid in the channel and hence, the effect of the change in conductivity with the increase in zeta potential is less prominent. Equivalently, when $n_r > 1$, the increase in zeta potential affects the streaming current more prominently and this is the reason why that as n_r increases, the location of the maxima shifts towards higher zeta potential. To summarize, at low n_r, the sensitivity of the streaming potential is larger towards the zeta potential. The location of the maxima shifts towards higher magnitudes of zeta potential as the n_r increases. The reason for these observations lies in the relative enhancement of the streaming current and the fluid conductivity.

Soft Matter Accepted Manuscript

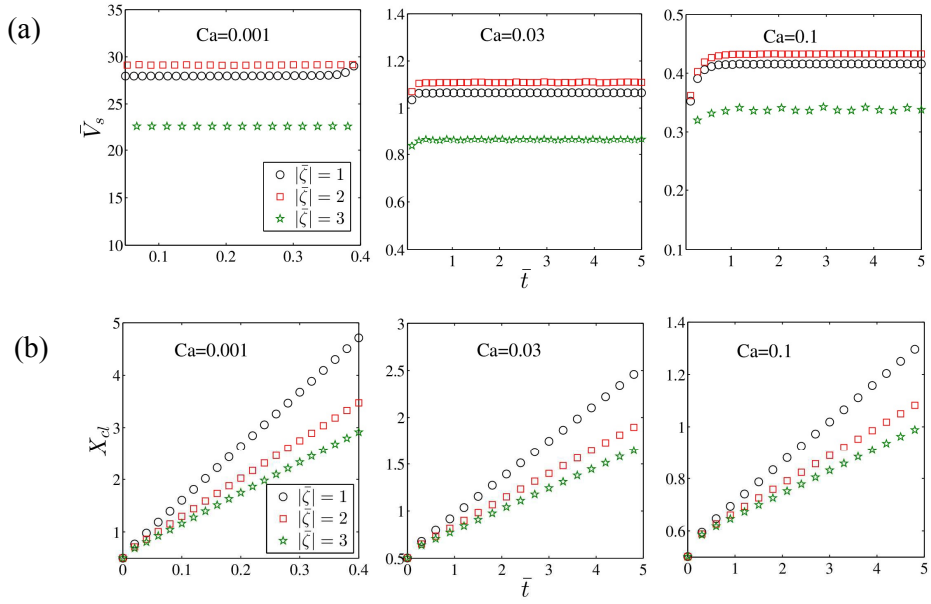

FIG. 6. (a) Temporal variation of the contact line location and (b) temporal variation of the induced streaming potential plotted for various $|\zeta|$ and for different Ca (0.5, 1.0 and 2.0). Here we have considered $n_r = 1$, and $\theta_s = \pi/3$.

An important physical parameter which governs multiphase flows happens to be the surface tension between adjacent phases. It essentially dictates the force acting on the interface of the two phases; a lower value of surface tension allows it to deform easily owing to the lack of the restoring force. Noticeably, the dimensionless manifestation of the surface tension is through the capillary number (Ca) which is a measure of the viscous forces to the surface tension forces at the interface. A lower capillary number is an indication that the viscous forces are negligible compared to the surface tension. It is expected that for a lower Ca, one would obtain a larger capillary penetration for a given time instant owing to the reduced viscous resistance in comparison to the driving effect of the surface tension. The enhancement of the capillary filling at lower capillary number is clearly verified from figure 6. In general, the result of this is that the magnitude of the streaming potential is higher for lower Capillary numbers for a given zeta potential and n_r. This is readily attributable to the higher streaming current owing to the enhanced flow at larger surface tension forces.

4. Conclusions

In this work, we have considered the pressure driven transport of two immiscible fluids with mobile charges in both the constituent phases. The transport is electrokinetically modulated, i.e., the current due to the flow of ions leads to a back-electromotive force (back EMF) termed as the streaming potential which retards the pressure driven flow. We describe the capillary filling dynamics and the induced streaming potential by means of a phase-field

Soft Matter Accepted Manuscript

methodology. Through a general formulation of the channel conductivity, the overall electroneutrality is obtained thereby accounting for the contrasts in the conductivities of the two fluids. Both the aforementioned approaches yield results which are qualitatively and quantitatively in good agreement. The contrast in the bulk concentrations in the two fluids has a significant impact on the overall dynamics of the fluid. If the displacing fluid has a higher conductivity, due to a higher bulk concentration, than the displaced fluid, the initial penetration is slower as compared to the case when the displacing fluid has a lower conductivity. The streaming potential in such a case shows a gradual decreasing trend as the capillary fills. We also highlight the effect of the surface potential on the filling dynamics. It is then revealed later that the streaming potential peaks at a certain value of zeta potential for a given ratio of bulk concentrations (n_r). We also show that the peak is more prominent at lower n_r.

The results portrayed here are expected to shed light on various aspects of multiphase electrokinetics. The fundamental geometry assumed in this work may lay the foundation for a more general homogenized description of streaming potential in flows through porous media which are relevant for enhanced oil recovery processes.[54] Non-polar solvents containing charged species or even different concentration brines may be driven by an alternate brine solution resulting in large streaming currents leading to streaming potentials. From an energy harvesting outlook, one may employ alternating patches of high conducting and low conducting fluids to generate periodically varying streaming potentials. Moreover, the presence of the interface acts as an assisting body force to the pressure gradient which opens up avenues for passive electrokinetic conversion.[55]

Acknowledgements

The authors gratefully acknowledge the financial support provided by SRIC, IIT Kharagpur, under the Projects “Centre of Excellence for Training and Research in Microfluidics”, and “Plant on a Chip”, for executing this work.

REFERENCES

1 J. C. T. Eijkel and A. van den Berg, *Lab Chip*, 2006, **6**, 1405–8.

2 M. D. Jackson, *J. Geophys. Res.*, 2008, **113**, B04201.

3 R. Schoch, J. Han and P. Renaud, *Rev. Mod. Phys.*, 2008, **80**, 839–883.

4 H. A. Stone, A. D. Stroock and A. Ajdari, *Annu. Rev. Fluid Mech.*, 2004, **36**, 381–411.

5 K. H. Jensen, D. L. Mullendore, N. M. Holbrook, T. Bohr, M. Knoblauch and H. Bruus, *Front. Plant Sci.*, 2012, **3**, 151.

6 K. H. Jensen, J. Lee, T. Bohr, H. Bruus, N. M. Holbrook and M. A. Zwieniecki, *J. R. Soc. Interface*, 2011, **8**, 1155–65.

7 M. D. Jackson, *J. Geophys. Res.*, 2010, **115**, B07206–B07222.

8 A. Revil and P. Leroy, *J. Geophys. Res.*, 2004, **109**, B03208.

Soft Matter Accepted Manuscript

9 A. Revil, *Geophys. Res. Lett.*, 2004, **31**, L11605.

10 J. H. Masliyah and S. Bhattacharjee, *Electrokinetic and Colloid Transport Phenomena*, John Wiley & Sons, Inc., Hoboken, NJ, USA, 2006.

11 S. H. Behrens and D. G. Grier, *J. Chem. Phys.*, 2001, **115**, 6716.

12 R. J. Hunter and L. R. White, *Foundations of colloid science*, Clarendon Press, London, 1989.

13 H. Bruus, *Theoretical microfluidics*, Oxford University Press, London, 2008.

14 L. Benson, L.-H. Yeh, T.-H. Chou and S. Qian, *Soft Matter*, 2013, **9**, 9767.

15 U. Mukherjee, J. Chakraborty and S. Chakraborty, *Soft Matter*, 2013, **9**, 1562–1569.

16 S. Levine and G. H. Neale, *J. Colloid Interface Sci.*, 1974, **47**, 520–529.

17 Z. Brož and N. Epstein, *J. Colloid Interface Sci.*, 1976, **56**, 605–612.

18 J. Lyklema and J. T. . Overbeek, *J. Colloid Sci.*, 1961, **16**, 501–512.

19 C. Zhao and C. Yang, *Adv. Colloid Interface Sci.*, 2013, **201-202**, 94–108.

20 S. Chanda, S. Sinha and S. Das, *Soft Matter*, 2014, **10**, 7558–7568.

21 S. Das, S. Mitra and S. Chakraborty, *Phys. Rev. E*, 2012, **86**, 011603.

22 D. Burgreen and F. R. Nakache, *J. Phys. Chem.*, 1964, **68**, 1084–1091.

23 A. V Delgado, F. González-Caballero, R. J. Hunter, L. K. Koopal and J. Lyklema, *J. Colloid Interface Sci.*, 2007, **309**, 194–224.

24 P. Vainshtein and C. Gutfinger, *J. Micromechanics Microengineering*, 2002, **12**, 252–256.

25 M. R. Davidson, R. P. Bharti and D. J. E. Harvie, *Chem. Eng. Sci.*, 2010, **65**, 6259.

26 M. Wang, C. C. Chang and R. J. Yang, *J. Chem. Phys.*, 2010, **132**, 024701–024706.

27 N. Vasu and S. De, *Int. J. Eng. Sci.*, 2010, **48**, 1641–1658.

28 A. Bandopadhyay, P. Goswami and S. Chakraborty, *J. Chem. Phys.*, 2013, **139**, 224503.

29 V.-N. Phan, C. Yang and N.-T. Nguyen, *Microfluid. Nanofluidics*, 2009, **7**, 519–530.

30 S. Das, S. Chanda, J. C. T. Eijkel, N. R. Tas, S. Chakraborty and S. K. Mitra, *Phys. Rev. E*, 2014, **90**, 043011.

31 J. D. Sherwood, *Phys. Fluids*, 2009, **21**, 013101.

32 D. Yang, M. Krasowska, C. Priest and J. Ralston, *Phys. Chem. Chem. Phys.*, 2014, **16**, 24473–24478.

33 R. Hunter, *Zeta potential in colloid science : principles and applications*, Academic Press, London ;New York, 1981.

34 L. Jouniaux and J.-P. Pozzi, *Geophys. Res. Lett.*, 1995, **22**, 485–488.

35 F. D. Morgan, E. R. Williams and T. R. Madden, *J. Geophys. Res.*, 1989, **94**, 12449–12461.

36 P. Antraygues and M. Aubert, *J. Geophys. Res.*, 1993, **98**, 22273.

Soft Matter Accepted Manuscript

37 A. Bandopadhyay, D. DasGupta, S. K. Mitra and S. Chakraborty, *J. Comput. Phys.*, 2015.

38 P. K. Mondal, U. Ghosh, A. Bandopadhyay, D. DasGupta and S. Chakraborty, *Phys. Rev. E*, 2013, **88**, 023022.

39 P. K. Mondal, U. Ghosh, A. Bandopadhyay, D. DasGupta and S. Chakraborty, *Soft Matter*, 2014, **10**, 8512–23.

40 S. Mandal, U. Ghosh, A. Bandopadhyay and S. Chakraborty, *J. Fluid Mech.*, 2015, **776**, 390–429.

41 J. Chakraborty and S. Chakraborty, 2014, pp. 339–353.

42 V. E. Badalassi, H. D. Ceniceros and S. Banerjee, *J. Comput. Phys.*, 2003, **190**, 371–397.

43 H. Ding, M. N. H. Gilani and P. D. M. Spelt, *J. Fluid Mech.*, 2010, **644**, 217.

44 R. Borcia and M. Bestehorn, *Phys. Rev. E*, 2007, **75**, 1–5.

45 F. H. J. van Der Heyden, D. Stein, K. Besteman, S. G. Lemay and C. Dekker, *Phys. Rev. Lett.*, 2006, **96**, 224502–224505.

46 S. Chakraborty, *Phys. Rev. Lett.*, 2007, **99**, 094504–094507.

47 P. Yue, C. Zhou and J. J. Feng, *J. Fluid Mech.*, 2010, **645**, 279.

48 D. Jacqmin, *J. Comput. Phys.*, 1999, **155**, 96–127.

49 P. Yue, C. Zhou, J. J. Feng, C. F. Ollivier-Gooch and H. H. Hu, *J. Comput. Phys.*, 2006, **219**, 47–67.

50 P. Yue, J. J. Feng, C. Liu and J. Shen, *J. Fluid Mech.*, 2004, **515**, 293–317.

51 C. Davidson and X. Xuan, *Electrophoresis*, 2008, **29**, 1125–1130.

52 C. Davidson and X. Xuan, *J. Power Sources*, 2008, **179**, 297–300.

53 S. Levine, J. . Marriott, G. Neale and N. Epstein, *J. Colloid Interface Sci.*, 1975, **52**, 136–149.

54 A. Bandopadhyay, D. DasGupta, S. K. Mitra and S. Chakraborty, *Phys. Rev. E*, 2013, **87**, 033006.

55 J. D. Sherwood, Y. Xie, A. Berg and J. C. T. Eijkel, *Microfluid. Nanofluidics*, 2013, **15**, 347–359.

Soft Matter Accepted Manuscript

GRAPHICAL TOC

A general framework for electrokinetic transport of two immiscible fluids in narrow confinements with different conductivities is developed.

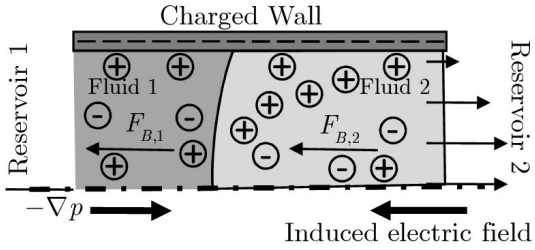

Soft Matter Accepted Manuscript